X-ray diffraction measurements for expanded liquid mercury in the metallic region

1991 J. Phys.: Condens. Matter 3 4443

(http://iopscience.iop.org/0953-8984/3/24/014)

J. Phys.: Condens. Matter 3 (1991) 4443–4457. Printed in the UK

X-ray diffraction measurements for expanded liquid mercury in the metallic region

Shinya Hosokawa, Tadashi Matsuoka and Kozaburo Tamura
Faculty of Integrated Arts and Sciences, Hiroshima University, Hiroshima 730, Japan

Received 10 December 1990, in final form 8 March 1991

Abstract. The x-ray diffraction measurements for expanded liquid Hg have been carried out for the first time in the density range from 13.55 to 10.26 g cm^{-3}, covering almost all of the metallic region of expanded liquid Hg. We have developed a new type of high pressure vessel and a new sample cell made of single-crystal sapphire for the x-ray diffraction measurements using the energy-dispersive method. We have obtained the structure factor and the pair distribution function as functions of density. It was found that the nearest-neighbour distance remains almost constant increasing slightly, less than 1%, with the reduction of density by about 24%. On the contrary, the coordination number decreases substantially and almost linearly with decreasing density. The volume expansion of liquid Hg in the metallic region is not accompanied by a uniform increase of interatomic distance but is mainly caused by a decrease of coordination number.

1. Introduction

A great deal of effort has been devoted to the study of the electronic and thermodynamic properties of fluid Hg over ranges of temperature and pressure sufficiently wide to include the liquid–gas critical point (critical data of Hg [1]: $T_c = 1478$ °C, $p_c = 1673$ bar, $d_c = 5.8$ g cm^{-3}). Much of the effort has been concerned with the metal–non-metal (M–NM) transition which occurs in the liquid when it is expanded beyond the critical point. A number of measurements of physical properties, including electrical conductivity [2–5], thermopower [3, 6–8], the Hall coefficient [9], optical reflectivity [10, 11], NMR [12], sound velocity [13] and the equation of state [1, 2, 4, 5] show that, as the density is reduced, the M–NM transition starts to occur at a density of about 9 g cm^{-3}.

Theoretical attempts have also been made to reach an understanding of the nature of the M–NM transition. Several band-structure calculations have been carried out for hypothetical forms of crystalline Hg in the low-density limit. The first calculation was by Devillers and Ross [14], who applied the pseudopotential method to calculate the energy bands for crystalline Hg with BCC, FCC and rhombohedral structures. For each structure, they obtained a band gap at about 8.5 g cm^{-3}. Band-structure calculations for such uniformly expanded crystalline Hg were carried out by many others [15, 16]. An alternative approach is that of Mattheiss and Warren [17]. They assumed that the nearest-neighbour distance was constant, so the density variation in expanded liquid Hg was due entirely to changes in coordination number. They performed a series of augmented-plane-wave calculations for crystalline Hg with FCC (co-ordination number = 12), BCC (8), SC (6) and diamond (4) structures and a fixed nearest-neighbour

0953-8984/91/244443 + 15 $03.50

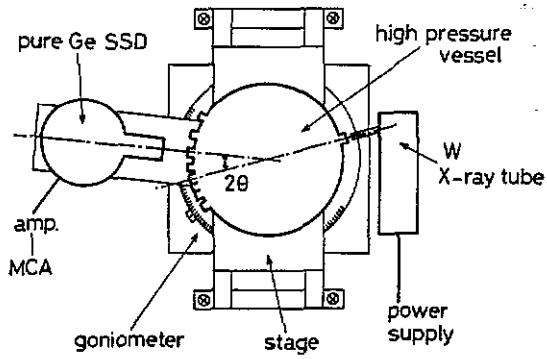

Figure 1. Schematic diagram of the energy-dispersive diffractometer.

distance. Their results showed a gradual development of the energy gap as the coordination number was reduced, although it was found necessary to increase the lattice constant by 1% to fully open a gap in tetrahedral coordination.

It is obvious that the structural data are important to the understanding of the mechanism of the M–NM transition of expanded liquid Hg. However, information on the structure of expanded liquid Hg is quite limited, despite rapid progress in understanding the electronic and thermodynamic properties. At present we have no experimental evidence to give a definite answer to the question of whether the interatomic distance increases uniformly with a fixed coordination number or that contrarily the coordination number decreases with a constant nearest-neighbour distance when liquid Hg is expanded.

In the present paper we report for the first time the structural data of expanded liquid Hg in the temperature and pressure range up to 1200 °C and 830 bar, in the density range 13.55 g cm^{-3}–10.26 g cm^{-3}, by the energy-dispersive x-ray diffraction method using new types of high pressure vessel and sample cell developed in our laboratory [18]. Experimental details and data analysis are presented in section 2. Structure factor and pair distribution function results are shown in section 3; also in section 3, we discuss the change in nearest-neighbour distance and coordination number with volume expansion.

2. Experiment

2.1. Constitution of the energy-dispersive diffractometer

We have carried out x-ray diffraction measurements for expanded liquid Hg using the energy-dispersive method. This technique has already been employed in our structural studies of expanded liquid Se near the liquid–gas critical point [18]. In the energy-dispersive method, white x-rays are used as the primary beam, and the scattered photons are detected and energy-analysed by a solid state detector (SSD) connected with a multichannel pulse-height analyser (MCA). Figure 1 shows the schematic diagram of the energy-dispersive diffractometer used in the present experiment. A horizontal goniometer system was adopted, in which an x-ray source and a detector were set in a horizontal plane. A fine-focus x-ray tube with a W target (Phillips Co Ltd, Model PW2284/20) was used and fixed at the position shown in the figure. The scattered x-rays

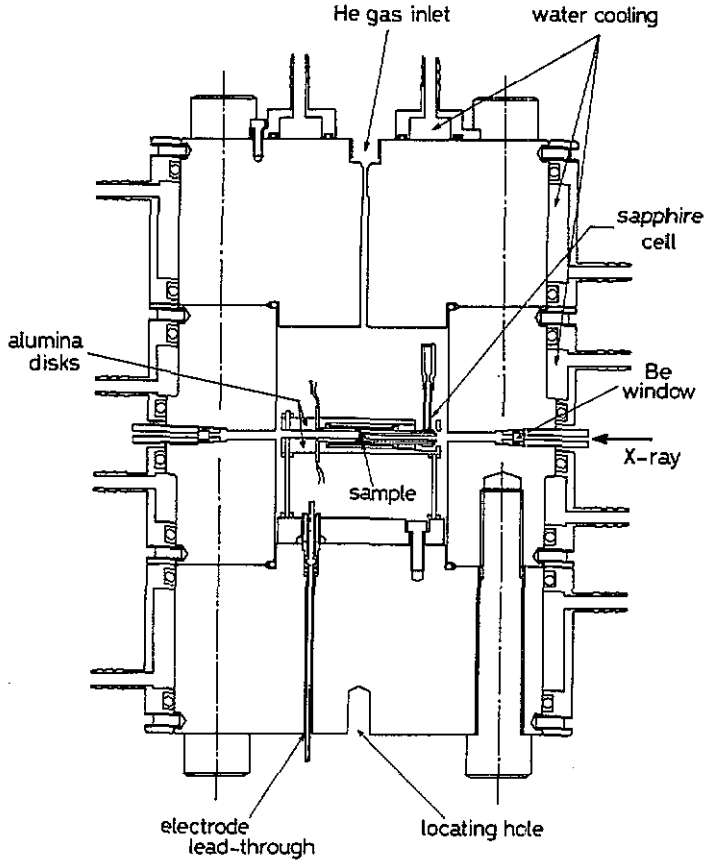

Figure 2. Side view of the high-pressure vessel for x-ray diffraction studies.

were detected by a pure Ge SSD (Canberra Industries Inc, Model PSR505), which was rotated around the vertical axis of the goniometer (Rigaku Co Ltd, Model 2155). Energy-dispersive measurements were performed at a fixed scattering angle 2θ and repeated at different angles in order to cover a sufficiently wide range of scattering wave number k, $k = (4\pi \sin \theta/hc)E$, E: photon energy, h: Planck constant, c: velocity of light. The position of the liquid sample contained in the sapphire cell, the details of which are described in the following section, was adjusted to be at the centre of the goniometer. The high-pressure vessel was placed on the stage laid across the goniometer. In the present experiment transmission geometry was employed.

2.2. High-pressure vessel

The experimental conditions of high temperatures, up to 1200 °C, and high pressures, up to 830 bar, were achieved with an internally heated high-pressure vessel made of a super-high-tension steel. Figure 2 shows the side view of the vessel which was constructed of a main cylinder with an inner diameter of 78 mm and two flanges. As seen in the figure, the sample was located at the centre of the high-pressure vessel and the alumina disks were used for holding the sapphire cell. The primary and scattered x-ray beams

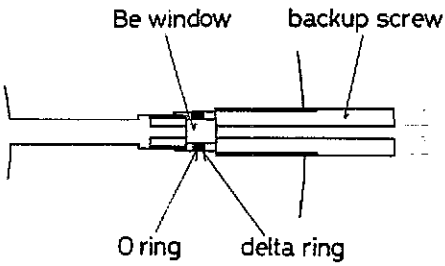

Figure 3. The construction around the Be window.

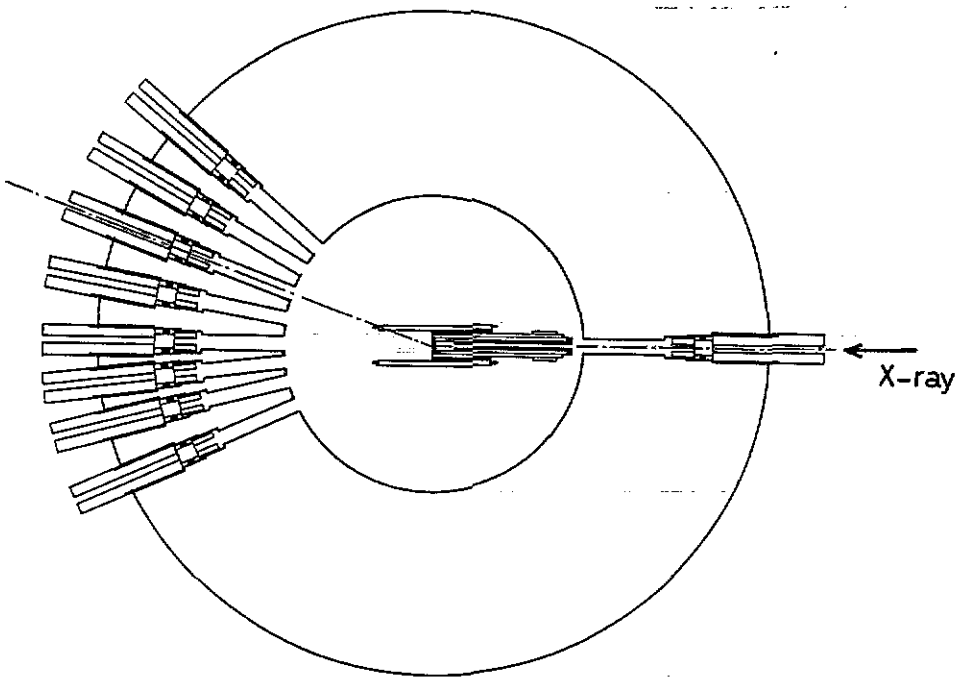

Figure 4. Top view of the high-pressure vessel for x-ray diffraction studies.

passed through beryllium windows with a thickness of 5 mm and diameter of 4 mm. Each of the Be windows was supported by the flat area of a backup screw, which is illustrated in figure 3. Figure 4 shows the top view of the vessel. As seen in the figure, there were nine windows, one of which was for the primary x-ray beam and the rest for the scattered ones. The windows for scattered x-ray beams were located at 2θ of 7, 10, 15, 19, 26, 29 and 39°. Special care was taken in adjusting the central axis of the vessel to that of the goniometer. For this, a locating hole was made in the centre of the lower flange as seen in figure 2. The electrodes for heaters and thermocouples were brought out of the vessel through the lower flange, where Bridgeman-type high-pressure seals were used. The vessel was pressurized by high purity grade (99.9999%) He gas which has a low absorption constant for x-rays in the energy range of the present experiment. Pressures were measured with a Heise gauge, having an accuracy of ±2 bar. Water cooling jackets were placed around the outside of the vessel.

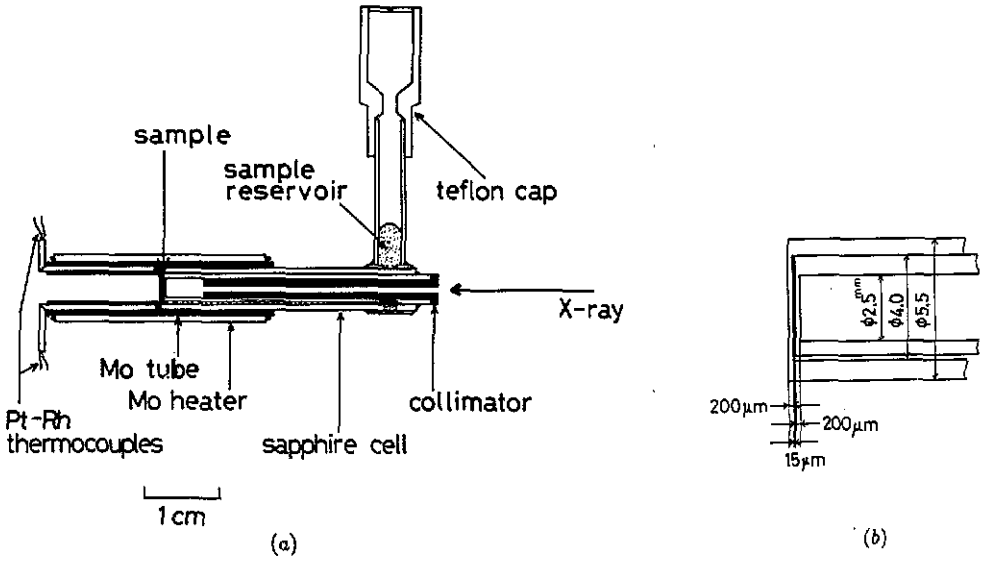

Figure 5. (*a*) The construction of the sapphire cell used for the x-ray diffraction studies of expanded liquid Hg. (*b*) Details of the sample space. For further details see text,

2.3. Sample cell

Expanded liquid Hg must be contained in a cell made of special material being transparent to x-rays and resistant to chemical corrosion by hot liquid Hg. A single-crystal sapphire cell was developed for the purpose, the details of which are illustrated in figure 5(*a*). The construction around the liquid sample is shown in figure 5(*b*) on an enlarged scale. A closed-end sapphire tube with inner diameter 2.5 mm, outer diameter 4 mm and length 36 mm was put into another closed-end tube with inner diameter 4 mm, outer diameter 5.5 mm and length 34 mm. The sample reservoir made of sapphire was connected to the outside of the tubes. The sapphire components were connected with a high-temperature glaze (Owens-Illinois Inc, Type 01328-C) providing a uniform gap between the closed ends of the tubes as shown in figure 5(*b*). The thickness of the closed end through which x-ray passed was 200 μm, and that of the gap was 15 μm. It is noticed that the thickness of liquid Hg should be very small because Hg has a high x-ray absorption coefficient in the present energy range.

In measuring x-ray diffraction from the liquid sample contained in the sapphire cell, the problem that must be overcome was to discriminate between the strong diffraction from the sapphire cell and that from the sample. This was overcome by employing the following procedure on assembling the cell. In the first step, both of the inner and outer closed-end tubes were manufactured so that their *c*-axes were parallel to the direction of the primary x-ray beam as shown in figure 5(*a*). When x-rays entered the tubes and were diffracted by the closed ends, Laue spots with a nearly triple symmetry were observed in the plane perpendicular to the *c*-axis. Each closed-end tube was turned independently around the *c*-axis until no Laue spots appeared in the horizontal direction. After that, the tubes were cemented. Since the SSD moved on the horizontal plane, the detected x-rays had no Bragg or coherent components originating from the sapphire cell.

The cell was heated by a heating element made of Mo wire with the diameter 0.5 mm. As seen in figure 5(*a*) the Mo heater was set around the Mo tube. It is noticed that a slit was made on the left hand side of the Mo tube so diffracted x-rays were able to go out through it. The temperature of the sample was measured by two Pt–30%Rh : Pt–6%Rh thermocouples which were located in the holes of Mo tube and were in close contact with the wall of the closed end of the outer sapphire tube. A collimator made of Mo with an inner diameter of 1.2 mm and a length of 31 mm was put into the inner closed-end tube as shown in the figure. The cell and the heater were supported by alumina disks as seen in figure 2. Special care was taken to construct the alumina disks so that the sample was precisely positioned at the centre of the goniometer. The space between the alumina disks and the inner wall of the vessel was filled with alumina powder to obtain good thermal insulation and to prevent convection of the compressed He gas.

The following procedure was followed to fill the sample space between the closed ends of the cell with liquid Hg. First, the liquid Hg sample was put into the Teflon cap, the largest inner-diameter of which was slightly larger than that of the spherically shaped liquid Hg sample. After closing the high-pressure seals, the entire assembly was evacuated. The high-pressure vessel was then pressurized using He gas at 2 or 3 bars that was sufficient to force liquid Hg through a small hole between the outer and inner sapphire tubes and fill the sample space. Once the cell had been filled, the temperature of the reservoir was maintained near room temperature. Pressure balance between the compressed liquid Hg pressure and the He pressure on the outside was achieved by making a small hole in the upper part of the Teflon cap. The purity of the Hg sample was 99.99%.

2.4. Measurement and data analysis

The diffracted x-ray photons from expanded liquid Hg at high temperatures and high pressures were collected at 2θ of 7, 10, 15, 19, 26 and 39°, by operating the x-ray tube at 50 kV and 25 mA. The spectrum in the energy region 17–42 keV was used for the analysis. The settings of $2\theta = 7$, 10, 15, 19, 26 and 39° correspond to the regions of $k =$ 1.05–2.60, 1.50–3.71, 2.25–5.56, 2.84–7.03, 3.88–9.58 and 5.75–14.21 $Å^{-1}$, respectively. As a result, the range of k in the present measurements was from 1.05 $Å^{-1}$ to 14.21 $Å^{-1}$.

The signals detected by SSD were accumulated in the MCA with 4096 channels. In order to obtain the relation of photon energy to channel number in the MCA, the fluorescent x-rays from Ni, Cu, Mo and Ag were observed. The channel numbers of these peaks in the MCA were fitted to the energies of the corresponding characteristic x-rays. The linear relationship between the photon energy and the channel number was quite good. The energy resolution of the SSD is about 200 eV. The obtained spectra were smoothed by averaging over 10 channels. An x-ray photon accumulating time at each scattering angle was 30 min.

In order to obtain the structure factor, $S(k)$, of expanded liquid Hg from the experimental scattering intensity, several data corrections had to be made, such as taking account of the effect of the detector, the energy spectrum of the primary x-ray beam, the energy dependence of the polarization on the primary beam, the absorption by the sapphire cell, compressed He gas, Be windows and liquid Hg itself, and finally Compton scattering from liquid Hg and the sapphire cell.

First we performed the correction for the escape-effect of the Ge SSD. The escape-effect occurs as follows. When a pure Ge SSD is used, some photons which come into the detector excite K core electrons of Ge atoms and produce K_α or K_β fluorescent x-rays

characteristic of Ge. If the fluorescent x-ray photon escapes from the detector, the pulse height from the detector decreases to the value corresponding to an energy smaller than the original photon energy. This causes the number of photons counted at the original photon energy to decrease, and that at the low energy to increase, with respect to the original numbers. The correction for such an escape effect was performed using the method reported by Nishikawa and Iijima [19]; this correction was very important in the present data analysis.

As is well known, in the x-ray diffraction measurements using the energy-dispersive method it is important to know the energy spectrum of the primary beam, $I_0(E)$. In the present experiment, $I_0(E)$ was determined by measuring the scattering from the empty sapphire cell with the same geometry around the cell and the same operating conditions of the x-ray tube as in the measurement of the sample. The measurement was carried out when the high pressure vessel was evacuated in advance of the sample measurement. As mentioned in sections 2 and 3, coherent scattering components originating from the sapphire cell were not included in the detected x-ray photons. Therefore, x-ray photons scattered from the sapphire contained only incoherent or Compton-scattered ones. The accumulated counts at certain channels corresponding to the photon energy E contain the counts of incoherently scattered photons that have incident energy E'. The measured intensity from the empty sapphire cell, $I_{cell}(E, \theta)$, is expressed as [19]

$$I_{cell}(E, \theta) = CK_{cell}(dE'/dE)I_{cell}^{incoh}(E', \theta)A_{cell}(E, E', \theta) \times A_{Be}(E, E')P(E', \theta)I_0(E'). \tag{2.1}$$

Note that $I_{cell}(E, \theta)$ is that obtained after the corrections for the escape-effect of the detector have been made. In (2.1), C is the scale factor to normalize the observed intensity to the calculated absolute intensity, K_{cell} is the Breit–Dirac recoil factor of the sapphire cell, I_{cell}^{incoh} is the incoherent scattering intensity from the sapphire cell, A_{Be} is the absorption factor of the Be windows, A_{cell} is the absorption factor of the sapphire cell and P is the polarization factor of the primary x-ray beam. Bonham [20] pointed out that the Breit–Dirac recoil factor for a system with bound electrons is E/E', and accordingly that the product $K_{cell}(dE'/dE)$ becomes E'/E. The value of I_{cell}^{incoh} was obtained as a sum of the calculated atomic incoherent scattering factors of constituent Al and O atoms [21]. The values of $A_{cell}(E, E', \theta)$ were calculated using the density, the mass absorption coefficient, the thickness of the sapphire cell and the Compton energy shift. The values of the mass absorption coefficient were taken from [22]. The values of $A_{Be}(E, E')$ were easily calculated. The polarization factor $P(E, \theta)$ is given as follows;

$$P(E, \theta) = (1 + \cos^2 \theta)/2 + (1 - \cos^2 \theta)\Pi(E)/2$$

where $\Pi(E)$ is the polarization of the primary x-ray beam. In the present analysis, it was permissible to neglect the second term because we adopted the data in the energy region below about 80% of the maximum photon energy [19]. Using these calculated values together with the observed energy spectra $I_{cell}(E, \theta)$ at 2θ of 7, 10, 15, 19, 26 and 39°, we obtained the spectrum of the primary beam multiplied by C. The value of $CI_0(E)$ is shown in figure 6.

We then measured the energy spectrum of x-rays scattered from liquid Hg contained in the sapphire cell. The structure factor, $S(k)$, of expanded liquid Hg was deduced according to the following procedure. The observed total spectrum $I_{obs}(E, \theta)$ is

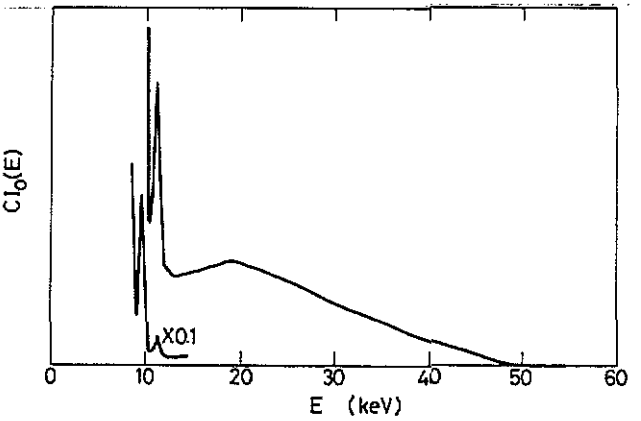

Figure 6. The energy spectrum of the primary x-ray beam obtained from the measurements for the empty sapphire cell.

expressed as [19],

$$\begin{aligned} I_{\rm obs}(E,\theta) = {} & CI^{\rm coh}_{\rm Hg}(E,\theta)A^{(1)}_{\rm Hg+cell}(E,\theta)A_{\rm He}(E)A_{\rm Be}(E)P(E,\theta)I_0(E) \\ & + CK_{\rm Hg}({\rm d}E'/{\rm d}E)I^{\rm incoh}_{\rm Hg}(E',\theta)A^{(2)}_{\rm Hg+cell}(E,E',\theta)A_{\rm He}(E,E') \\ & \times A_{\rm Be}(E,E')P(E',\theta)I_0(E') \\ & + CK_{\rm cell}({\rm d}E'/{\rm d}E)I^{\rm incoh}_{\rm cell}(E',\theta)A^{(3)}_{\rm Hg+cell}(E,E',\theta)A_{\rm He}(E,E') \\ & \times A_{\rm Be}(E,E')P(E',\theta)I_0(E') \end{aligned} \tag{2.2}$$

where the first term is the spectral intensity of the coherent scattering from the liquid Hg sample, the second term is the incoherent scattering from the liquid Hg sample and the third term is the incoherent scattering from the cell. It should be noticed that the term concerned with the coherent scattering from the sapphire cell does not appear in (2.2). The multiple scattering was not taken into account. In (2.2), C is the same scale factor as in (2.1), $I^{\rm coh}_{\rm Hg}(E,\theta)$ is the coherent scattering intensity of the liquid Hg sample, $K_{\rm Hg}$ is the Breit–Dirac recoil factor of Hg, $I^{\rm incoh}_{\rm Hg}(E',\theta)$ is the incoherent scattering intensity caused by the liquid Hg sample. The subscripts on the absorption factor A indicate that A is that of the Hg sample and the sapphire cell, He gas or Be window. The value of $A^{(1)}_{\rm Hg+cell}$ is the absorption factor indicating that x-ray photons coherently scattered in the liquid Hg sample are absorbed by both the cell and the sample itself in the process of scattering. The value of $A^{(2)}_{\rm Hg+cell}$ and $A^{(3)}_{\rm Hg+cell}$ are those for x-ray photons incoherently scattered in the sample and the cell, respectively. As already mentioned, E' is the initial photon energy, which is reduced to E after Compton scattering.

In order to obtain the coherent scattering component from the liquid Hg sample, we should eliminate the contribution of the incoherent scattering from both the sample and the sapphire cell. As seen in (2.2), the first term, namely the spectrum of the coherent scattering from the liquid Hg sample, was obtained by subtracting the second and the third terms from $I_{\rm obs}$. The Breit–Dirac recoil factor K is $(E/E')^2$ in the case of free electrons, and the ratio of the band width, $({\rm d}E'/{\rm d}E)$, cancels out the recoil factor, as pointed out by Egami [23]. In the present analysis $K_{\rm Hg}({\rm d}E'/{\rm d}E)$ was taken to be unity. The maximum difference between the values of K in the case of the bound and free

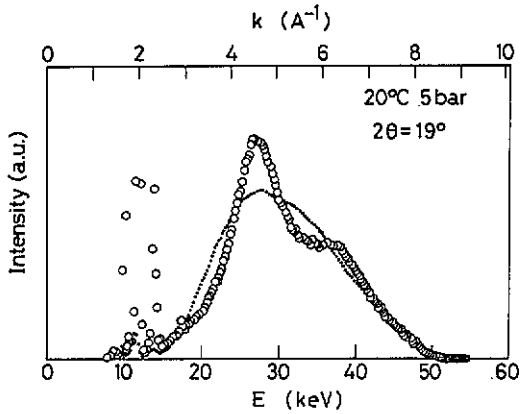

Figure 7. The intensity of coherent scattering from liquid Hg obtained from a measurement at 20 °C, 5 bar and at $2\theta = 19°$, which is expressed as the first term in (2.2) and indicated by empty circles. The full circles show the intensity of the self-scattering from the individual Hg atoms. The ratio of these two values gives the structure factor $S(k)$.

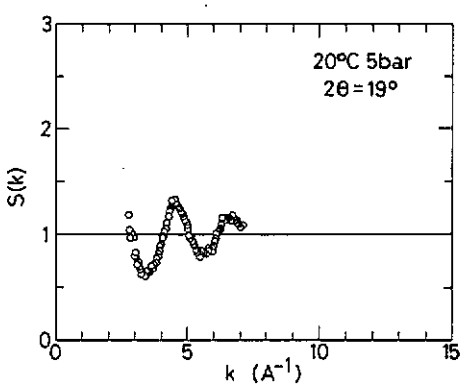

Figure 8. The structure factor, $S(k)$, of liquid Hg at 20 °C and 5 bar in the limited k-region corresponding to $2\theta = 19°$.

electron systems was estimated to be less than 2% in the present energy region, which gives a maximum deviation of 0.6% in the final results. The calculation of $I_{\mathrm{Hg}}^{\mathrm{incoh}}$ and $I_{\mathrm{cell}}^{\mathrm{incoh}}$ were made using the values of the atomic incoherent scattering factors of Hg, Al and O atoms [21, 24]. Estimations of A in the second and third terms were performed using data such as densities, mass absorption coefficients and thicknesses of the Hg sample, the cell, the He gas and the Be window. Since $CI_0(E)$ was given as in figure 6, we could calculate the second and the third terms. The maximum contribution of the incoherent scattering to the total intensity, I_{obs}, was about 40%. The first term obtained, that is the spectrum concerning the coherent scattering from the liquid Hg sample, is shown in figure 7 as empty circles, as an example for liquid Hg at 20 °C, 5 bar and $2\theta = 19°$. In the figure full circles show the calculated spectrum of the self-scattering from the individual Hg atoms expressed as

$$CI_{\mathrm{Hg}}^{\mathrm{self}}(E, \theta)A_{\mathrm{Hg+cell}}^{(1)}(E, \theta)A_{\mathrm{He}}(E)A_{\mathrm{Be}}(E)P(E, \theta)I_0(E)$$

where $I_{\mathrm{Hg}}^{\mathrm{self}}$ is the self-scattering intensity from the individual Hg atoms, namely $I_{\mathrm{Hg}}^{\mathrm{self}} = Nf^2$; N is the number of Hg atoms and f is the atomic scattering factor of an Hg atom. Using the data for f from [22], $I_{\mathrm{Hg}}^{\mathrm{self}}$ was easily obtained.

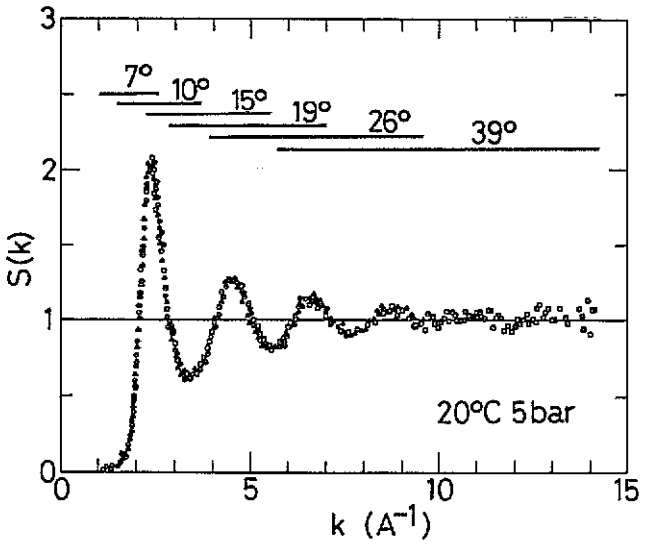

Figure 9. The structure factor, $S(k)$, of liquid Hg at 20 °C and 5 bar obtained for different angle settings. Empty circles show the data obtained for angle settings at $2\theta = 7$ and 19°, empty triangles show those at 10 and 26° and empty squares show those at 15 and 39°.

As is well known, I_{Hg}^{coh} appeared in the first term of (2.2) is expressed as $I_{Hg}^{coh} = Nf^2S(k)$. Therefore, $S(k)$ was easily obtained by calculating the ratio of the two values shown as empty and full circles in figure 7. Figure 8 shows $S(k)$ obtained at 20 °C, 5 bar and at $2\theta = 19°$. The $S(k)$ data obtained for different angle settings for liquid Hg at 20 °C and 5 bar are shown in figure 9. Empty circles show the $S(k)$ data obtained for angle settings of $2\theta = 7$ and 19°, empty triangles show those obtained for $2\theta = 10$ and 26° and empty squares show those obtained for $2\theta = 15$ and 39°. As seen in the figure, the consistency of the data in the same k-region is good. More detailed descriptions of the data analysis will be given elsewhere.

3. Results and discussion

We have carried out x-ray diffraction measurements for expanded liquid Hg in the temperature and pressure ranges up to 1200 °C and 830 bar along the saturated vapour-pressure curve and with densities ranging from 13.55 to 10.26 g cm^{-3}, so we surveyed almost all the metallic region of expanded Hg. Figure 10 shows the $S(k)$ of expanded liquid Hg at different temperatures and pressures. Dots represent the experimental data and the full curves show the Fourier transforms of the corresponding pair distribution functions, $g(R)$, which are shown in figure 11. In the region $k > 9$ Å^{-1}, the data are rather scattered because of the decrease of x-ray intensity with increasing scattering angle. Nevertheless, $S(k)$ at 20 °C and 5 bar is in good agreement with previous data obtained by the usual angle-dispersive method [25], except for a small difference between the amplitudes of the first peaks; this confirms the reliability of the data at high temperatures and high pressures.

The characteristic feature of the temperature and pressure variations of $S(k)$ is that the oscillation damps and the peak width becomes broad with increasing temperature

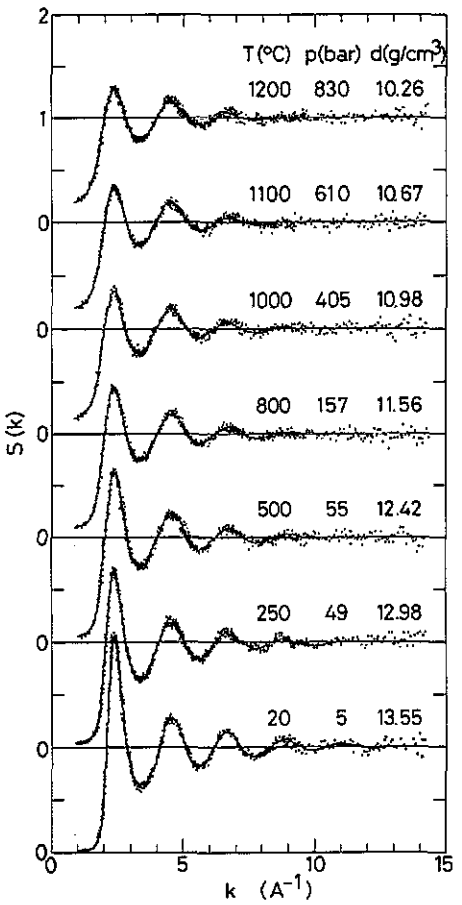

Figure 10. The structure factor, $S(k)$, of expanded liquid Hg. Temperature, pressure and density are indicated at the upper right hand side of each of the data points.

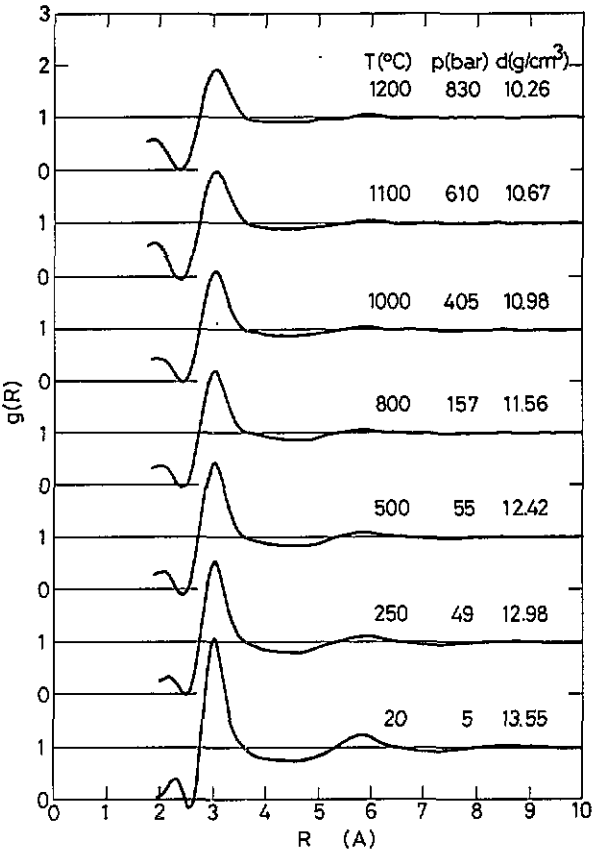

Figure 11. The pair distribution function, $g(R)$, of expanded liquid Hg. Temperature, pressure and density are shown at the upper right hand side of each of the data curves.

and pressure, or with decreasing density. This tendency is noticed in the first peak, whereas the second peak seems to damp rather slowly. The amplitude of the first maximum of $S(k)$, $S(k_1)$, normalized with that at the melting temperature, $S_{mp}(k_1)$, is plotted as a function of the reduced temperature in figure 12, together with those for some other liquid metals [26, 27]. Winter *et al* [26] pointed out that the temperature dependence of $S(k_1)/S_{mp}(k_1)$ has the universal tendency to be distinguished by a degree of valence. As clearly seen in figure 12, the plots for expanded liquid Hg do not lie on the curve for a monovalent alkali metal group, but on that for a polyvalent metal group.

Pair distribution functions, $g(R)$, deduced from the Fourier transformation of the structure factors, $S(k)$, are shown in figure 11. In the Fourier transformation, the values of $S(k)$ in the small-k region between 0 and 1.05 Å^{-1} were estimated by interpolating the values of $S(0)$ and $S(k)$ above 1.05 Å^{-1}, where the values of $S(0)$ were calculated using the experimentally obtained isothermal compressibility of expanded liquid Hg [1, 4]. The small peaks of $g(R)$ in the region of $R < 2.5$Å may be due to termination

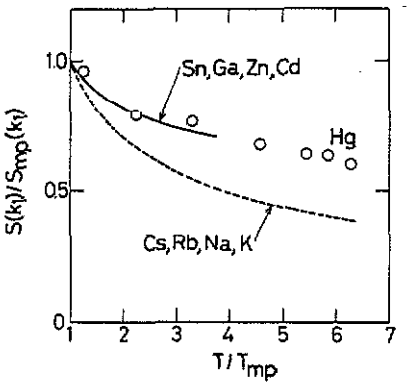

Figure 12. The height of the first maximum of $S(k)$ of expanded liquid Hg normalized with that at the melting temperature, $S(k_1)/S_{mp}(k_1)$, is plotted as a function of reduced temperature, T/T_{mp}, together with similar values for some other liquid metals [26, 27].

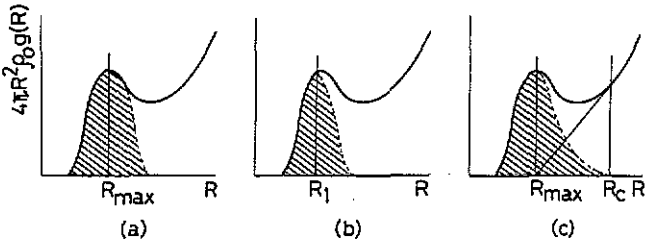

Figure 13. Three different methods of integration of the first peak of the radial distribution function $4\pi R^2\rho_0 g(R)$ in order to deduce the coordination number. See text for further details.

effects on the Fourier transformation. The data for $g(R)$ at 20 °C and 5 bar have several characteristic features: the first peak has an asymmetric shape, the first minimum is flat in the wide region from 4 Å to 5 Å and the second peak is rather small compared with those of simple liquid metals such as alkali metals. The data for $g(R)$ at 20 °C and 5 bar are in excellent agreement with the previous data [25]. With increasing temperature and pressure, that is with decreasing density, the oscillation of $g(R)$ diminishes. The broadening of the first peak gradually occurs but no remarkable change of the peak position is observed. The asymmetry of the first peak seems to remain even at high temperatures and pressures up to 1200 °C and 830 bar. The nearest-neighbour distance, R_1, obtained from the position of the first peak maximum of $g(R)$ is 3.03 Å at 20 °C and 5 bar, slightly longer than that of the crystal with rhombohedral form, and increases slightly, less than 1%, with a density reduction of about 24%. The second peak damps rapidly and its position hardly seems to change with the density decrease.

As is well known, it is not easy to obtain the definite coordination number from the diffusive and broad $g(R)$ pattern of the liquid state. Because there is usually considerable overlap between the first- and second-neighbour peaks, experimental values of coordination number depend quite sensitively on the method employed to define and integrate the first-neighbour peak. However, variations of coordination number as a function of temperature, pressure or density can be determined with more reliability as long as a consistent definition of the coordination number is used. We employed three different methods to define and integrate the first-neighbour peak. The first (method A) is the usual method, integrating the radial distribution function, $4\pi R^2\rho_0 g(R)$, up to the maximum position, R_{max}, and taking twice the integral to deduce N_1 as shown in figure 13(a), where ρ_0 denotes the average number density of Hg. The second (method B) is

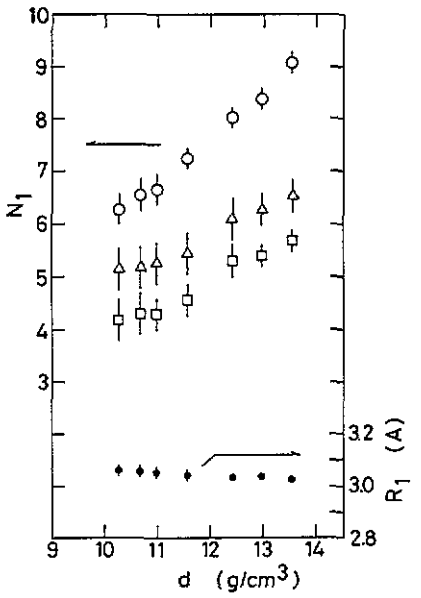

Figure 14. Coordination number, N_1, and first-neighbour distance, R_1, of expanded liquid Hg as a function of density. Empty triangles, squares and circles denote N_1 obtained using methods A, B and C, respectively. Full circles show the variation of R_1.

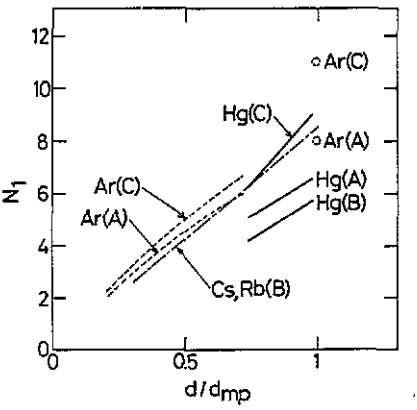

Figure 15. N_1 of expanded liquid Hg as a function of the reduced density, d/d_{mp}, together with those of expanded liquid monovalent alkali metals [26, 27] and liquid Ar [28], where d_{mp} is the density at the melting point. Note that the data are obtained using the three different methods mentioned for figure 13 and are plotted together.

the method integrating $4\pi R^2\rho_0 g(R)$ up to the maximum position of $g(R)$, R_1, and then taking twice the integral as shown in figure 13(*b*). Method B was used for expanded liquid alkali metals by Hensel's group [26, 27]. The last (method C) is a special method taking account of the asymmetry of the first-neighbour peak. In method C, we draw a tangential straight line from the first-peak position, R_{max}, towards the first minimum of $4\pi R^2\rho_0 g(R)$, as shown in figure 13(*c*). We regard the triangle area below the tangent line as that due to the penetration of the second neighbours, and subtract it.

The coordination numbers N_1 obtained by these calculations are plotted in figure 14 as a function of density, together with the nearest-neighbour distance, R_1. Uncertainties in these values are indicated by error bars. At 20 °C and 5 bar, N_1 of liquid Hg is 6.5 by method A, 5.7 by method B and 9.1 by method C. As is clearly seen in figure 14, N_1 decreases linearly with decreasing density whatever method might be employed. The decrease of density by about 24% in liquid Hg causes N_1 to decrease by 19–31%. From these results we conclude that the volume-expansion of liquid Hg in the metallic region is not of the type of 'a uniform expansion with a fixed coordination number' but is caused by 'a decrease of coordination number with a fixed nearest-neighbour distance'. It is interesting to study whether this tendency continues or not when one goes across the M–NM transition region where the density becomes less than 9 g cm^{-3}.

Figure 15 shows N_1 of liquid Hg as a function of reduced density, which is normalized with that at the melting point, together with those of expanded liquid monovalent alkali metals [26, 27] and liquid Ar [28]. Note that different methods are employed to deduce N_1 for each element. Despite these liquid elements having different valencies and

different effective interatomic potentials, N_1 for each element shows similar density variation; the position of the main peak in $g(R)$ remains virtually unchanged over the ranges investigated, whereas the value of N_1 tends to decrease almost linearly with decreasing density. It is of interest to study the reason the variations of N_1 and R_1 with decreasing density seem to be the same for various liquid elements. Structural data for other expanded liquid metals should be accumulated, especially in the wide-density region. The x-ray diffraction measurement for expanded liquid Hg extending to the low-density region, less than 9 g cm^{-3}, where the M–NM transition takes place is now in progress.

Acknowledgments

The authors are grateful to Professors M Watabe and K Hoshino for helpful discussions in the present study. Rigaku Co Ltd and High Pressure Chemical Co Ltd are acknowledged for their technical support concerning the x-ray apparatus and the high-pressure vessel, respectively. This work is partly supported by the Grant-in-Aid for Scientific Research Fund from the Ministry of Education, Science and Culture of Japan.

References

[1] Götzlaff W, Schönherr G and Hensel F 1988 *Z. Phys., Chem.–NF* **156** 219
Götzlaff W 1988 *PhD Thesis* University of Marburg
[2] Hensel F and Frank E U 1966 *Ber. Bunsenges. Phys. Chem.* **70** 1154
[3] Schmutzler R W and Hensel F 1972 *Ber. Bunsenges. Phys. Chem.* **76** 531
[4] Schönherr G, Schmutzler R W and Hensel F 1979 *Phil. Mag.* B **40** 411
[5] Yao M and Endo H 1982 *J. Phys. Soc. Japan* **51** 966
[6] Duckers L J and Ross R G 1972 *Phys. Lett.* A **38** 291
[7] Neale F E and Cusack N E 1979 *J. Phys. F: Met. Phys.* **9** 85
[8] Yao M and Endo H 1982 *J. Phys. Soc. Japan* **51** 1504
[9] Even U and Jortner J 1972 *Phil. Mag.* **25** 715; 1973 *Phys. Rev.* B **8** 2536
[10] Ikezi H, Schwarzenegger K, Simons A L, Passner A L and McCall S L 1978 *Phys. Rev.* B **18** 2494
[11] Hefner W, Schmutzler R W and Hensel F 1980 *J. Physique Coll.* **41** C8–62
[12] El-Hanany U and Warren W W Jr 1975 *Phys. Rev. Lett.* **34** 1276
[13] Suzuki K, Inutake M, Fujiwaka S, Yao M and Endo H 1980 *J. Physique Coll.* **41** C8–66
[14] Devillers M A C and Ross R G 1975 *J. Phys. F: Met. Phys.* **5** 73
[15] Overhof H, Uchtmann H and Hensel F 1976 *J. Phys. F: Met. Phys.* **6** 523
[16] Fritzson P and Berggren K-F 1976 *Solid State Commun.* **19** 385
[17] Mattheiss L F and Warren W W Jr 1977 *Phys. Rev.* B **16** 624
[18] Tamura K 1990 *J. Non-Cryst. Solids* **117/118** 450
[19] Nishikawa K and Iijima T 1984 *Bull. Chem. Soc. Japan* **57** 1750
[20] Bonham R A 1981 *Phys. Rev.* A **23** 2950
[21] Cromer D T 1969 *J. Chem. Phys.* **50** 4857
[22] MacGillavry C H and Rieck G D (ed) 1962 *International Tables for X-ray Crystallography* vol III (Birmingham: Kynoch) pp 175–92, 202–7
[23] Egami T 1978 *J. Mater. Sci.* **13** 2587
[24] Cromer D T and Mann J B 1967 *J. Chem. Phys.* **47** 1892
[25] Bosio L, Cortes R and Segaud C 1979 *J. Chem. Phys.* **71** 3595
There are many records of structural data for liquid Hg at room temperature using the angular- and energy-dispersive x-ray diffraction as mentioned below . We find small discrepancies among them.
Black P J and Cundall J A 1965 *Acta Crystallogr.* **19** 807
Kaplow R, Strong S L and Averbach B L 1965 *Phys. Rev.* A **138** 1336

Rivlin V G, Waghorne R M and Williams G I 1966 *Phil. Mag.* **13** 1169
Halder N C and Wagner C N J 1968 *Z. Naturforsch.* a **23** 992
Caputi R W, Rodriquez S E and Pings C J 1968 *Phys. Chem. Liquids* **1** 121
Waseda Y and Suzuki K 1970 *Phys. Status Solidi* **40** 183
Ruppersberg H and Reiter 1972 *Acta Crystallogr.* A **28** 233
Prober J M and Schultz J M 1975 *J. Appl. Cryst.* **8** 405
[26] Winter R, Hensel F, Bodensteiner T and Gläser W 1987 *Ber. Bunsenges. Phys. Chem.* **91** 1327
[27] Franz G, Freyland W, Gläser W, Hensel F and Schneider E 1980 *J. Physique Coll.* **41** C8–194
Franz G 1980 *PhD Thesis* University of Marburg
[28] Mikolaj P G and Ping C J 1967 *J. Chem. Phys.* **46** 1401
Gingrich N S and Tompson C W 1962 *J. Chem. Phys.* **36** 2398